Published in final edited form as:

Mol Cancer Ther. 2018 January ; 17(1): 264–275. doi:10.1158/1535-7163.MCT-17-0407.

Metabolite profiling reveals the glutathione biosynthetic pathway as a therapeutic target in triple negative breast cancer

Alexander Beatty[1], **Lauren S. Fink**[1], **Tanu Singh**[1], **Alexander Strigun**[2], **Erik Peter**[2], **Christina M. Ferrer**[3], **Emmanuelle Nicolas**[1], **Kathy Q. Cai**[1], **Timothy P. Moran**[1], **Mauricio J. Reginato**[3], **Ulrike Rennefahrt**[2], and **Jeffrey R. Peterson**[1]

[1]Fox Chase Cancer Center, 333 Cottman Avenue, Philadelphia, PA 19111

[2]metanomics GmbH & Metanomics Health GmbH, Tegeler Weg 33, 10589 Berlin, Germany

[3]Department of Biochemistry & Molecular Biology, Drexel College of Medicine, Philadelphia, PA

Abstract

Cancer cells can exhibit altered dependency on specific metabolic pathways and targeting these dependencies is a promising therapeutic strategy. Triple negative breast cancer (TNBC) is an aggressive and genomically heterogeneous subset of breast cancer that is resistant to existing targeted therapies. To identify metabolic pathway dependencies in TNBC, we first conducted mass spectrometry-based metabolomics of TNBC and control cells. Relative levels of intracellular metabolites distinguished TNBC from non-transformed breast epithelia and revealed two metabolic subtypes within TNBC that correlate with markers of basal-like versus non-basal-like status. Among the distinguishing metabolites, levels of the cellular redox buffer glutathione were lower in TNBC cell lines compared to controls and markedly lower in non-basal-like TNBC. Significantly, these cell lines showed enhanced sensitivity to pharmacological inhibition of glutathione biosynthesis that was rescued by N-acetylcysteine, demonstrating a dependence on glutathione production to suppress ROS and support tumor cell survival. Consistent with this, patients whose tumors express elevated levels of γ–glutamylcysteine ligase, the rate-limiting enzyme in glutathione biosynthesis, had significantly poorer survival. We find, further, that agents that limit the availability of glutathione precursors enhance both glutathione depletion and TNBC cell killing by γ–glutamylcysteine ligase inhibitors *in vitro*. Importantly, we demonstrate the ability to this approach to suppress glutathione levels and TNBC xenograft growth *in vivo*. Overall, these findings support the potential of targeting the glutathione biosynthetic pathway as a therapeutic strategy in TNBC and identify the non-basal-like subset as most likely to respond.

Keywords

Triple-negative breast cancer; metabolomics; glutathione; glutaminase

Corresponding author: Jeffrey R. Peterson, Fox Chase Cancer Center, 333 Cottman Ave., Philadelphia, PA 19111. Phone: 215-728-3568, Jeffrey.Peterson@fccc.edu.

Introduction

Metabolic reprogramming is regarded as a hallmark of cancer that contributes to the progression of the disease (1). Differential metabolic requirements for rapidly proliferating malignant cells relative to non-transformed counterparts suggest that targeting metabolism may be a potential strategy for developing novel cancer therapies (2–4). A pivotal step in developing new therapeutic approaches that exploit metabolic vulnerabilities is to identify metabolic alterations that are relevant for a particular malignancy. Advances in the field of metabolomics have made it possible to measure a broad spectrum of cellular metabolites, providing an approach to identify the specific metabolic alterations associated with cancer (5, 6).

TNBC represents ~15–20% of all breast cancers but does not express the estrogen (ER) or progesterone receptor (PR) and lacks HER2 amplification, and, consequently, is not responsive to current targeted therapies. Thus, TNBC represents an unmet medical need and the standard of care for TNBC has remained relatively stagnant for many years. Cytotoxic chemotherapy is the primary treatment modality and while chemotherapy has a fairly high response rate, the likelihood of relapse is substantial (7). Here, we use broad-spectrum metabolite profiling in TNBC to subtype the disease based on metabolic heterogeneity and identify potential metabolic targets that can be exploited therapeutically.

Materials and Methods

Cell lines and materials

Nine of the 12 TNBC cell lines, as well as the non-transformed, immortalized control breast cell line MCF10A were obtained from the American Type Culture Collection (ATCC, Manassas, VA 20110, USA). Excluding BT-20 and MDA-MB-231, which were received in 2012, the cell lines were received in 2011. MDA-MB-468, BT-474, and ZR-75-1 were obtained by the Cell Culture Facility at Fox Chase Cancer Center from ATCC as part of the NCI-60 panel. The NCI-60 panel was obtained in 2003. The two additional TNBC cell lines, CAL-148 and MFM-223, were purchased from the Deutsche Sammlung von Mikroorganismen und Zellkulturen GmbH (Braunschweig, Germany) in 2011. The suppliers routinely authenticate the cell lines by short tandem repeat profiling though the cell lines were not authenticated by our laboratory. All cell lines were amplified and frozen within 2 months of receipt. Cell lines are periodically tested for *Mycoplasma* contamination using DAPI (4′,6-diamidino-2-phenylindole) to stain DNA. Two different primary human mammary epithelial cell (HMEC) isolates were obtained from GIBCO (Details A10565) and Lonza (CC-2551), respectively, in 2012. Culture media for the cell lines can be found in Supplementary Table S1.

Metabolite Profiling and Normalization

Cells (5–6 biological replicates) were harvested at a density of ~ 70–80% at either 24 or 48 hours after seeding to lumox plates (Sarstedt) as previously described (8). Cells were washed twice with 0.9% NaCl and extracted in dichloromethane:ethanol (0.82:1) as previously described (9). Extracts were flash frozen in liquid nitrogen according to (10). Samples were

analyzed by gas chromatography-mass spectrometry (MS) and liquid chromatography-MS/MS as described elsewhere (11).

Metabolite profiling data were normalized against the median in the pooled reference sample (generated by pooling samples from additional biological replicates collected from all investigated cell lines) to give Pool-normalized ratios (performed for each sample per metabolite) to compensate for inter- and intra-instrumental variability. Samples were also subjected to internal sample normalization to the median metabolite signal for each sample to account for differences in the amount of applied sample material.

Metabolomics Statistical Analysis

Multivariate statistical analysis was performed using Simca P+ software v13.0 (Umetrics, Umea, Sweden) on the z-scores of the metabolites. All metabolite data were $\log_{10}$-transformed (to ensure an approximate normal distribution), centered and scaled to unit variance. Scaling to unit variance introduced a common scale for all metabolites independent of their absolute variance. Hierarchical clustering was conducted using R.utils and Hmisc within the statistical software package R (version 2.8.1). The algorithm for the calculation of the hierarchical clustering with stability information was taken from the pvclust-package (12). Hierarchical clustering used Ward's method using the Spearman correlation between the metabolic profiles to determine the similarity between samples. Univariate "one-metabolite-at-a-time" analysis was performed by analysis of variance (ANOVA), conducted using R with package nlme (13).

qPCR

Total RNA was isolated using an RNeasy kit (Qiagen) and reverse transcribed using Moloney murine leukemia virus reverse transcriptase (Ambion). Taqman gene expression assays (Life Technologies) were used to amplify KRT5 (Hs00361185_m1), KRT14 (Hs00265033_m1), KRT17 (Hs01588578_m1), KRT23 (Hs00210096_m1) cDNA. POLR2F was used as normalizer (F: TGCCATGAAGGAACTCAAGG, R:TCATAGCTCCCATCTGGCAG). The slopes of the standard curves used to convert cycle threshold values to quantities were between −3.2 and −3.7 cycle/log decade.

Viability assays

Compounds were added 24 hours after cell plating and viability was assessed at the specified time point using the CellTiter-Glo luminescent cell viability assay (Promega) according to the manufacturer's instructions. Data were normalized to vehicle-treated controls and IC_{50} curves were generated using Graphpad Prism. Viability assays were generally performed at least twice. In assays that included N-acetylcysteine (Sigma-Aldrich) treatment, the medium was replaced every 48 hours except in RNAi experiments where additional N-acetylcysteine was added every 48 hours. CB-839 was obtained from Focus Biomolecules (14). Erastin was purchased from Cayman Chemical (15), and BPTES was acquired from Sigma (16).

siRNA

Transfections (DharmaFECT 1, Thermo Scientific) for siRNA knockdown experiments used ON_TARGETplus SMART pools (Thermo Scientific) for *GCLC* and *GCLM*, or a non-

targeting siRNA pool (Dharmacon). Protein knockdown was assessed 72 hours post-transfection using specific antibodies [GCLM (NBMP1-33405, Novus Bio) and GCLC (M01, clone 3H1, H00002729-M01 Abnova)].

Glutathione measurements

Total glutathione (reduced plus oxidized forms) was quantified using the GSH/GSSG-Glo kit (Promega) according to the manufacturer's instructions. When comparing glutathione levels for various drug treatments, samples were normalized to parallel cell viability measurements using the CellTiter-Glo assay (Promega). For tumor samples, 50–100 mg of tissue was homogenized in ice-cold phosphate-buffered saline using dounce homogenizer. The homogenate was diluted 7-fold and added to an equal volume of total glutathione lysis reagent. The remainder of the assay was carried out using the manufacturer's instructions.

ROS measurements

Cellular ROS levels were measured using CellROX green reagent (ThermoFisher Scientific) according to the manufacturer's instructions. Fields of fixed cells to be imaged were selected at random. Fluorescent micrographs were captured with a Nikon Eclipse TE2000 inverted microscope using Ocular software (QImaging). Image quantification was performed using ImageJ (NIH).

Mouse xenografts

Orthotopic xenografts were generated by implanting 2.5 million MDA-MB-231 cells in 100 μL phosphate-buffered saline (PBS) mixed with 100 μL growth factor-reduced Matrigel (Corning) into the fourth inguinal fat pad of four- to six-week-old female NOD.*Cg-Prkdc*^{scid}*Il2rg*^{tm1Wjl}/SzJ (NSG) mice. After 14 days, animals were randomized into treatment groups. L-BSO (Sigma) was administered via the drinking water (20 mM) *ad libitum* as previously reported (17, 18). Vehicle (control group) or 200 mg/kg sulfasalazine (Sigma) in 0.1 N NaOH (pH 7.5) was dosed by intraperitoneal injection once daily. Vehicle or CB-839 was delivered twice daily by intraperitoneal injection at a dose of 10mg/kg in a solution of 25% (w/v) hydroxypropyl-β-cyclodextrin (Roquette) in PBS. The Fox Chase Cancer Center Institutional Animal Care and Use Committee approved all animal procedures.

Tissue preparation, histology, immunohistochemistry

Tumor sections were fixed in 10% formalin for 24–48 hours, dehydrated and embedded in paraffin. Immunohistochemical staining was carried out using standard methods. Sections were incubated overnight with primary antibodies to anti-human Ki-67 (Clone MIB-1, DAKO) and cleaved caspase-3 (Cell Signaling; #9661) at 4 °C in a humidified chamber. Micrographs were taken with a Nikon DS-Fi1 camera (Melville, NY, USA) on a Nikon Eclipse 50i microscope and quantified using a ScanScope CS5 slide scanner (Aperio).

Results

Metabolite profiling reveals two major TNBC metabolic subtypes

We used untargeted mass-spectrometry-based metabolite profiling to examine relative levels of cell-associated metabolites in a panel of 15 TNBC cell lines and non-cancerous controls. To capture the diversity of TNBC phenotypes, 12 widely studied cell lines were chosen that included representatives from each of the six gene expression-based subtypes of TNBC defined previously (19). Control cells were the immortalized but non-transformed MCF10A breast epithelial cell line and two independent isolates of primary human mammary epithelial cells (HMEC). Proliferating cell cultures were rapidly harvested, extracted, and intracellular metabolites were quantified. We conducted unsupervised hierarchical clustering based on 155 robustly quantifiable metabolites to examine the relationship among the cell lines (Fig. 1A). Replicate measurements of the same cell line clustered more closely together than any two cell lines, demonstrating that biological variation between cell types exceeds variation among replicates (Fig. 1B; larger version in Fig. S1). Cells clustered into three metabolic subtypes (MSTs), with control cells (MST1) segregating from two TNBC cell line clusters (MST2 and MST3) (Fig. 1B). Co-clustering of the immortalized control cell line MCF10A with the primary HMEC cells suggests that the metabolic distinction between cancer versus non-transformed, proliferating cells is more significant than that between immortalized and primary cells.

We conducted principal component analysis to evaluate inter- and intra-cell line variability (Fig. 1C). HMEC cells were excluded from this model due to their extreme segregation from the remaining cell lines. We generally observed close clustering among replicates demonstrating technical robustness of the measurements. Second, we observed a strong segregation of the MCF10A control cells (black) from the TNBC cell lines (Fig. 1C), suggesting a prominent distinction in the metabolic phenotype of cancer versus control cells.

To independently assess the robustness of the metabolic subtypes defined by hierarchical clustering, we performed an additional principal component analysis on the replicate measurements from all 15 cell types (TNBC and controls) (Fig. 1D). MST1 cells (black) clearly segregated from the TNBC cell lines, though the HMECs and MCF10A clustered independently, perhaps reflecting metabolic differences between primary and immortalized control cells, respectively. In addition, the distinction between MST2 and MST3 was preserved in this analysis, consistent with the hierarchical clustering analysis. Overall, this subtyping analysis revealed that TNBC cells are metabolically distinct from non-transformed breast epithelia, and identified two major TNBC metabolic subtypes.

TNBC metabolic subtypes are distinguished by expression of basal cytokeratins

To identify genes differentially expressed between the two TNBC metabolic subtypes, we examined publicly available gene expression data (GSE10890) that included ten of the TNBC cell lines in our panel. The most differentially expressed gene was *KRT5* (cytokeratin 5), which had significantly higher expression (adjusted p=0.000025) in cell lines of MST3 than MST2 (Fig. S2A). Quantitative RT-PCR confirmed higher expression of *KRT5* in MST3 (Fig. 1E; Welch's t-test, p=0.002). Cytokeratin 5 is a clinically relevant marker that is

used to distinguish basal-like from non-basal-like breast cancers (20, 21), suggesting that the metabolic subtypes might segregate according to basal-like status. This hypothesis was supported by mRNA expression of additional basal cytokeratins (*KRT14, KRT17, KRT23*), which were more highly expressed in MST3 than MST2 (Fig. 1E; Fisher's combined probability test, one-tailed, p=0.00038). Furthermore, we compared the MST group membership of each cell line to its gene expression-based subtype as defined by Pietenpol and coworkers (19) and found that MST2 was enriched for non-basal-like (mesenchymal, mesenchymal stem-like, luminal androgen receptor, unclassified) gene-expression subtypes while MST3 correlated with basal-like (basal-like 1, basal-like 2, immunomodulatory) subtypes (Fig S2B; Fisher's exact test, p=0.046). Taken together, these observations support an underlying metabolic basis for the distinction between basal-like and non-basal-like TNBC.

Metabolites distinguishing the metabolic subtypes

We examined metabolites driving the separation of the MSTs by performing an ANOVA to compare the relative levels of individual metabolites in each subtype. Comparing the TNBC MSTs (MST2 & MST3) to the non-cancerous MST1 revealed several metabolites that distinguished cancer from normal epithelial cells (Fig. 2A, 2B, complete data provided in Table S3). Among the most increased metabolites in TNBC compared to control were polyunsaturated fatty acids including docosahexaenoic acid, arachidonic acid, and dihomo-gamma-linolenic acid. The most decreased metabolites in TNBC included the branched chain amino acids valine and leucine as well as the aromatic amino acid tryptophan (Fig. 2A, 2B).

The reduced form of the antioxidant glutathione was the metabolite with the largest difference in abundance between MST2 & MST3 (Fig. 2C, Table S3). Furthermore, both TNBC MSTs had lower levels of glutathione relative to non-transformed cells (MST1) (Fig. 2D). MST2 had on average 15.3-fold lower glutathione, and MST3 had 2.4-fold lower glutathione relative to MST1. The reduced:oxidized glutathione balance (GSH:GSSG) was also significantly lower in MST2 compared to MST3 (Fig. S3A), though the NADPH/NAP^+ ratio was not significantly different when measured separately (Fig. S3B). The levels of the glutathione precursors cysteine and glutamate were also lower in MST2 relative to MST3 by 2.5-fold and 1.7-fold, respectively (Fig. 2C, Table S3). Finally, 5-oxoproline, a metabolite involved in glutathione salvage, was lower in TNBC (both MST2 & MST3) compared to MST1, with MST2 again exhibiting a more robust decrease (Fig. 2C, Table S3). These observations demonstrate lower glutathione and its precursors in TNBC, particularly in MST2 and are consistent with elevated oxidative stress.

Glutathione biosynthesis is required to suppress ROS in TNBC cells and is associated with poor patient prognosis

We hypothesized that low glutathione in TNBC, and particularly in MST2, reflected dependence on glutathione biosynthesis to maintain adequate antioxidant capacity. To test this, we measured the effect of buthionine sulphoximine (BSO) on cell viability across the panel. BSO irreversibly inhibits γ-glutamylcysteine ligase (GCL), the first and rate-limiting enzyme in glutathione biosynthesis, leading to rapid depletion in cellular glutathione (Fig.

S3C) (22). Consistent with our hypothesis, the average half-maximal inhibitory concentration (IC_{50}) for BSO in cell lines of MST2 was significantly lower compared to the other subtypes (Fig. 3A; Welch's t-test, p=0.01). MST3 showed intermediate sensitivity to BSO, while the MST1 cell line MCF10A was relatively resistant. Confirming that BSO toxicity is a result of inadequate redox buffering capacity, the thiol-based ROS scavenger N-acetylcysteine suppressed the decreased viability associated with BSO treatment in multiple cell lines (Fig. 3B and supplemental Fig S3D). Additionally, the sensitivity of the cell lines to BSO correlated significantly with sensitivity to an exogenous source of ROS, hydrogen peroxide (Spearman correlation, p=0.006, Fig. 3C). Furthermore, MST2 cells showed increased ROS levels compared to MST3 cells (Figs. 3D & 3E), which could be reduced by N-acetylcysteine (Fig. S3E), consistent with increased ROS stress. We also assessed BSO toxicity in two non-TNBC breast cancer cell lines. While the luminal B subtype cell line BT474 was largely resistant to BSO, the luminal A cell line ZR-75-1 was BSO-sensitive (Fig. S3F), suggesting that glutathione-dependence may not be exclusive to TNBC. Nevertheless, we observed an addiction to glutathione biosynthesis in TNBC cell lines of MST2.

Additionally, we performed siRNA knockdown of the gene encoding either the catalytic (*GCLC*) or modulatory (*GCLM*) subunit of GCL in representative MST2 cell lines. Transient transfection with the corresponding siRNA resulted in significant protein reduction at 72 hours (Fig. 3F and Fig. S4A), but only a moderate decrease in glutathione at this time point (Fig. S4B). While neither siRNA treatment was sufficient to significantly reduce cell viability (Fig. S4A), knockdown of *GCLC* (Fig. 3F), but not *GCLM* (Fig. S4C) was synthetically lethal with low dose BSO. To examine the relationship between glutathione depletion and loss of cell viability, we analyzed the effect of BSO dose on glutathione levels and cell viability in representative BSO-resistant (HCC1806) and sensitive (MDA-MB-231) TNBC cell lines. While HCC1806 cells did not exhibit a loss of cell viability until glutathione levels were decreased to ~2% of control levels, MDA-MB-231 cells began to show decreased cell viability when glutathione levels were lowered to ~12% (Fig. 3G). Thus, BSO resistance reflects diminished glutathione dependence, rather than inability of BSO to deplete glutathione in these cells.

To gain insight into the potential clinical relevance of glutathione dependence in breast cancer, we evaluated *GCLC/GCLM* expression in breast tumors from The Cancer Genome Atlas Research Network (23). Using the cBioportal analysis tool (24, 25), we found that 13% (123/960) of all breast cancer samples had copy number amplification or overexpression of either *GCLC* or *GCLM* and this was increased to 25% (25/99) in the triple-negative subset. Importantly, *GCLC/GCLM* amplification or overexpression was associated with shorter disease-free survival (p=0.006, Fig. 4, left) and overall survival (p=0.00038, Fig. 4, right), consistent with a selection for increased glutathione biosynthesis in order to support tumorigenesis.

Combinatorial approaches to suppress glutathione biosynthesis reduce tumor cell growth *in vitro* and *in vivo*

Glutathione is a non-ribosomally synthesized tri-peptide composed of glutamate, cysteine and glycine. Glutamate and cysteine are substrates for the first and rate-limiting step in glutathione biosynthesis (Fig. 5A). Based on the sensitivity of TNBC cells to glutathione depletion, we hypothesized that limiting the availability of these amino acid precursors may enhance BSO toxicity. Inhibitors of the cystine/glutamate antiporter xCT sulfasalazine (SASP) and erastin were used to limit cysteine availability (26, 27). System xCT transports cystine into the cell, in exchange for glutamate, where it is converted to cysteine that can be utilized for glutathione biosynthesis and other functions. Additionally, xCT inhibitors may lower cellular glutathione by promoting glutathione secretion (28). To limit glutamate, we used small-molecule inhibitors of glutaminase (CB-839 and BPTES) (14, 16). Glutaminase deaminates glutamine into glutamate, which can be used for glutathione biosynthesis and for xCT-mediated cystine uptake in addition to anaplerosis of the citric acid cycle (29).

The combination of CB-839 with BSO, at doses at which the individual agents had minimal effect on cell viability, induced cell death in the non-basal-like MDA-MB-231 cells and also in the basal-like HCC1806 cells (Fig. 5B). Furthermore, sub-toxic doses of BSO in MDA-MB-231 potentiated toxicity of BPTES (Fig. 5C) or erastin (Fig. 5D) by over 100-fold and 10-fold, respectively. To quantitatively evaluate these combinations, we systematically measured the effect of sub-toxic BSO on the potency of glutaminase inhibitors and xCT inhibitors in both non-basal-like (red) and basal-like (blue) TNBC cell lines using CellTiter-Glo viability assays (Fig. 5E, complete dose-response curves in Fig. S5A and S5B). CB-839 and BPTES more selectively enhanced BSO in the non-basal-like cells and we investigated whether this was associated with glutamine-dependence and/or a further reduction in glutathione levels. We cultured representative cell lines in media containing increasingly lower amounts of glutamine (Fig. 5F). Strikingly, MDA-MB-468 cells were insensitive to glutamine depletion and this correlated with the lack of BSO enhancement by CB-839 and BPTES (Fig. 5E). Conversely, glutamine-dependence of the other cell lines correlated with enhancement of BSO toxicity by glutaminase inhibitors. Furthermore, glutamine depletion significantly reduced cellular glutathione levels (Fig. 5G), suggesting that glutamine and glutaminase activity are required, in part, to maintain cellular glutathione levels. Consistent with this model, BSO toxicity was enhanced when cells were cultured under reduced glutamine conditions (Figs. 5H & I) and the toxicity of CB-839 could be partially suppressed by the antioxidant N-acetylcysteine (Fig. 5J).

While sensitizing BSO doses generally enhanced the potency of inhibitors of glutaminase and xCT, some cell lines showed strong BSO interactions with only one of the two amino acid precursor pathways (e.g. HCC1806 and MDA-MB-468). This allowed us to test whether the differential sensitivity to glutaminase and xCT inhibitors is associated with their differential ability to deplete glutathione in each cell line. Consistent with this hypothesis, in HCC1806 cells, CB-839 and BSO, but not erastin and BSO, resulted in a significantly lower level of total glutathione compared to BSO treatment alone (Student’s t-test, p=0.008) (Fig. 5K). Conversely, in MDA-MBA-468 cells, erastin and BSO significantly enhanced glutathione depletion compared to BSO alone (p=0.038), whereas CB-839 plus BSO did not

(Fig. 5L). These data support the hypothesis that the enhanced growth suppression by these combinations is due to glutathione depletion and suggest that different cell lines may exhibit different limiting substrates for glutathione biosynthesis. Limiting substrate was not predicted by the relative expression level of glutaminase (GLS1) or the xCT subunit SLC7A11 measured previously (30). By contrast, BSO toxicity was significantly enhanced by both SASP and CB-839 in MDA-MB-231 cells (Fig. 5M). The enhancement of BSO by these compounds was selective because in a screen of 23 inhibitors of metabolic enzymes, the toxicity of only 3 compounds were enhanced by BSO by >2 fold and the most strongly enhanced of these was SASP (Fig. S5C).

We next investigated whether these combinations could suppress the growth of orthotopic MDA-MB-231 xenografts. Consistent with previous studies (31), BSO as a single agent showed no tumor suppression activity (Fig. 6A). However, treatment of tumor-bearing mice with 20 mM BSO (in the drinking water) only suppressed tumor total glutathione to 39±7% of control levels (Fig. 6B) while suppression of glutathione by >85% was required to trigger loss of MDA-MB-231 cell viability *in vitro* (Fig. 3G). The combination of BSO and CB-839 did not further suppress glutathione levels over BSO alone (Fig. S5F) and also did not suppress tumor growth (Figs. S5D and S5E), though this may be due to inadequate glutaminase inhibition because CB-839 was administered at a lower dose than in prior reports (14, 32). Alternatively, the lack of activity may reflect a differential requirement for glutamine created by the *in vivo* environment (33, 34). Consistent with the combined ability of BSO plus SASP to reduce glutathione levels in cultured cells (Fig. 5M), mice treated with this combination had 25% of the glutathione of control-treated mice after 7 days of treatment (Fig. 6C) and, importantly, grew more slowly (Fig. 6D) and had smaller tumor masses (Fig. 6E) at the end of the experiment, consistent with a previous report (31). Treated mice did exhibit weight loss compared to controls, however (Fig. 6F). Tumors treated with BSO and SASP showed fewer Ki67-positive cells compared to control tumors (41±2% vs. 55±3%, Student's t-test, $p=4.1\times10^{-9}$), and both these groups showed little to no staining for an apoptotic marker (cleaved caspase 3; 0.1% of cells in both groups) (Fig. 6G). These findings support the ability of co-treatment with BSO and SASP to reduce glutathione synthesis over BSO alone and reduce tumor growth *in vivo*.

Discussion

We applied broad-spectrum metabolomics to identify metabolic dependencies in TNBC, leading to four main insights into this poorly understood cancer. First, we observe two distinct metabolic phenotypes within TNBC that each differ from that of untransformed mammary epithelial cells. Second, the two TNBC metabolic subtypes correlate significantly with clinically relevant markers of basal-like status. Third, non-basal-like TNBC cells generally exhibit a relatively greater reliance on glutathione biosynthesis that can be targeted by the clinical agent BSO. Fourth, we have identified rational drug combinations that have the potential to robustly improve treatment efficacy and broaden the applicability of anti-glutathione therapy in TNBC (31). Overall, our work demonstrates how untargeted metabolomic analysis can identify differentially expressed metabolites that reflect underlying cancer-specific metabolic pathway dependencies that can point toward new therapeutic strategies. In addition, our data support an emerging and important distinction

between basal-like and non-basal-like TNBC (35) and provides a metabolomics resource for the discovery of additional metabolic adaptations that support the proliferation of each subtype.

The metabolites that we identified as distinguishing TNBC cells from non-transformed breast epithelial cells were largely consistent with previous studies (36–39). Importantly, most of these studies were performed using primary breast tumor tissue, suggesting that the TNBC cell line panel accurately recapitulated metabolic alterations observed *in vivo*. The polyunsaturated fatty acids docosahexaenoic acid (DHA) and arachidonic acid (AA) were elevated in TNBC, in agreement with reports that DHA and AA are increased in primary breast tumors (36, 37). β-alanine, a breakdown product of pyrimidines and carnosine, was also elevated in TNBC as reported for ER-negative breast cancer (38). Additionally, we identified decreases in a number of amino acids, particularly branched chain amino acids, in TNBC, consistent with increased amino acid catabolism. A decrease in tryptophan is consistent with increased expression and activity of indoleamine 2,3 dioxygenase (IDO), the rate-limiting enzyme in tryptophan catabolism that produces the immunomodulatory metabolite kynurenine. Kynurenine and IDO are increased in ER/PR-negative compared to ER-positive breast tumors (39).

TNBC cell lines, particularly those of MST2, exhibited alterations consistent with elevated oxidative stress. Most notably, the redox buffer reduced glutathione was decreased in TNBC cell lines, and robustly decreased in MST2. Low glutathione may reflect a reduced ability of TNBC to maintain adequate glutathione reserves relative to elevated demand for redox buffering capacity. Interestingly, our results differ from previous clinical studies reporting that reduced glutathione levels were generally increased in numerous cancer types including breast (40). Additionally, breast tumors, and specifically ER/PR-negative tumors, exhibited elevated glutathione (39). This discrepancy may reflect a specific feature of non-basal-like TNBC, a subtype that was not specifically characterized in the prior studies, or could reflect the influence of non-cell-autonomous factors on glutathione levels *in vivo*.

Our finding that TNBC is sensitive to anti-glutathione therapy is consistent with recent publications (14, 41, 42). Two of these studies identified a dependence of TNBC on availability of the glutathione precursors glutamate and cysteine, respectively (14, 42). TNBC cell lines were sensitive to glutaminase inhibitor, CB-839, which suppressed tumor growth *in vivo* (14). Similarly, the cysteine/glutamate antiporter xCT inhibitor sulfasalazine robustly inhibited proliferation, decreased glutathione content, and increased ROS levels (42). Our results suggest that the effects of CB-839 and sulfasalazine may be at least partially mediated by restricting glutathione biosynthesis.

Several agents designed to exacerbate oxidative stress in cancer cells and promote cell death are in preclinical or clinical development (43). Here, we present an approach to stratify TNBC to predict which will be most responsive to anti-glutathione therapeutics. Unexpectedly, the metabolic subtypes that we defined correlated with basal-like versus non-basal-like TNBC. Because basal-like status is routinely determined by immunohistochemical staining of tumor biopsies, existing clinical practice can be used to stratify TNBC patients and potentially identify those most likely to respond to therapy targeting glutathione

biosynthesis. Furthermore, the correlation between metabolic subtype and basal-like status suggests that similar metabolic distinctions could exist in other cancers that are divided into basal-like and non-basal-like types.

Supplementary Material

Refer to Web version on PubMed Central for supplementary material.

Acknowledgments

We gratefully acknowledge Drs. Balachandran, Golemis and Connolly for comments on the manuscript. We gratefully acknowledge the financial support of the Pennsylvania Breast Cancer Coalition, the Rita Holman Foundation, the Joseph C. Romano Trust Fund, a FCCC-TU Interdisciplinary Translational Cancer Research Award and NIH grants GM083025 and CA006927.

References

1. Hanahan D, Weinberg RA. Hallmarks of cancer: the next generation. Cell. 2011; 144(5):646–674. [PubMed: 21376230]
2. Galluzzi L, Kepp O, Vander Heiden MG, Kroemer G. Metabolic targets for cancer therapy. Nature reviews Drug discovery. 2013; 12(11):829–846. [PubMed: 24113830]
3. Tennant DA, Duran RV, Gottlieb E. Targeting metabolic transformation for cancer therapy. Nature reviews Cancer. 2010; 10(4):267–277. [PubMed: 20300106]
4. Stine ZE, Walton ZE, Altman BJ, Hsieh AL, Dang CV. MYC, Metabolism, and Cancer. Cancer Discov. 2015; 5(10):1024–1039. [PubMed: 26382145]
5. Jung K, Reszka R, Kamlage B, Bethan B, Stephan C, Lein M, et al. Tissue metabolite profiling identifies differentiating and prognostic biomarkers for prostate carcinoma. International journal of cancer Journal international du cancer. 2013; 133(12):2914–2924. [PubMed: 23737455]
6. Vermeersch KA, Styczynski MP. Applications of metabolomics in cancer research. Journal of carcinogenesis. 2013; 12:9. [PubMed: 23858297]
7. Engebraaten O, Vollan HK, Borresen-Dale AL. Triple-negative breast cancer and the need for new therapeutic targets. Am J Pathol. 2013; 183(4):1064–1074. [PubMed: 23920327]
8. Daemen A, Peterson D, Sahu N, McCord R, Du X, Liu B, et al. Metabolite profiling stratifies pancreatic ductal adenocarcinomas into subtypes with distinct sensitivities to metabolic inhibitors. Proc Natl Acad Sci U S A. 2015; 112(32):E4410–4417. [PubMed: 26216984]
9. Bordag N, Janakiraman V, Nachtigall J, Gonzalez Maldonado S, Bethan B, Laine JP, et al. Fast Filtration of Bacterial or Mammalian Suspension Cell Cultures for Optimal Metabolomics Results. PLoS One. 2016; 11(7):e0159389. [PubMed: 27438065]
10. Czech C, Berndt P, Busch K, Schmitz O, Wiemer J, Most V, et al. Metabolite profiling of Alzheimer's disease cerebrospinal fluid. PLoS One. 2012; 7(2):e31501. [PubMed: 22359596]
11. van Ravenzwaay B, Cunha GC, Leibold E, Looser R, Mellert W, Prokoudine A, et al. The use of metabolomics for the discovery of new biomarkers of effect. Toxicol Lett. 2007; 172(1–2):21–28. [PubMed: 17614222]
12. Suzuki R, Shimodaira H. Pvclust: an R package for assessing the uncertainty in hierarchical clustering. Bioinformatics. 2006; 22(12):1540–1542. [PubMed: 16595560]
13. Pinheiro, JBD.DebRoy, S.Sarkar, D., R Core Team. , editors. nlme: Linear and Nonlinear Mixed Effects Models. https://cran.r-project.org/package=nlme2017 [cited 2017]
14. Gross MI, Demo SD, Dennison JB, Chen L, Chernov-Rogan T, Goyal B, et al. Antitumor activity of the glutaminase inhibitor CB-839 in triple-negative breast cancer. Mol Cancer Ther. 2014; 13(4):890–901. [PubMed: 24523301]
15. Yagoda N, von Rechenberg M, Zaganjor E, Bauer AJ, Yang WS, Fridman DJ, et al. RAS-RAF-MEK-dependent oxidative cell death involving voltage-dependent anion channels. Nature. 2007; 447(7146):864–868. [PubMed: 17568748]

16. Robinson MM, McBryant SJ, Tsukamoto T, Rojas C, Ferraris DV, Hamilton SK, et al. Novel mechanism of inhibition of rat kidney-type glutaminase by bis-2-(5-phenylacetamido-1,2,4-thiadiazol-2-yl)ethyl sulfide (BPTES). The Biochemical journal. 2007; 406(3):407–414. [PubMed: 17581113]
17. Watanabe T, Sagisaka H, Arakawa S, Shibaya Y, Watanabe M, Igarashi I, et al. A novel model of continuous depletion of glutathione in mice treated with L-buthionine (S,R)-sulfoximine. The Journal of toxicological sciences. 2003; 28(5):455–469. [PubMed: 14746349]
18. Griffith OW, Meister A. Potent and specific inhibition of glutathione synthesis by buthionine sulfoximine (S-n-butyl homocysteine sulfoximine). J Biol Chem. 1979; 254(16):7558–7560. [PubMed: 38242]
19. Lehmann BD, Bauer JA, Chen X, Sanders ME, Chakravarthy AB, Shyr Y, et al. Identification of human triple-negative breast cancer subtypes and preclinical models for selection of targeted therapies. J Clin Invest. 2011; 121(7):2750–2767. [PubMed: 21633166]
20. van de Rijn M, Perou CM, Tibshirani R, Haas P, Kallioniemi O, Kononen J, et al. Expression of cytokeratins 17 and 5 identifies a group of breast carcinomas with poor clinical outcome. Am J Pathol. 2002; 161(6):1991–1996. [PubMed: 12466114]
21. Cheang MC, Voduc D, Bajdik C, Leung S, McKinney S, Chia SK, et al. Basal-like breast cancer defined by five biomarkers has superior prognostic value than triple-negative phenotype. Clin Cancer Res. 2008; 14(5):1368–1376. [PubMed: 18316557]
22. Griffith OW, Meister A. Glutathione: interorgan translocation, turnover, and metabolism. Proc Natl Acad Sci U S A. 1979; 76(11):5606–5610. [PubMed: 42902]
23. Ciriello G, Gatza ML, Beck AH, Wilkerson MD, Rhie SK, Pastore A, et al. Comprehensive Molecular Portraits of Invasive Lobular Breast Cancer. Cell. 2015; 163(2):506–519. [PubMed: 26451490]
24. Gao J, Aksoy BA, Dogrusoz U, Dresdner G, Gross B, Sumer SO, et al. Integrative analysis of complex cancer genomics and clinical profiles using the cBioPortal. Science signaling. 2013; 6(269):pl1. [PubMed: 23550210]
25. Cerami E, Gao J, Dogrusoz U, Gross BE, Sumer SO, Aksoy BA, et al. The cBio cancer genomics portal: an open platform for exploring multidimensional cancer genomics data. Cancer Discov. 2012; 2(5):401–404. [PubMed: 22588877]
26. Gout PW, Buckley AR, Simms CR, Bruchovsky N. Sulfasalazine, a potent suppressor of lymphoma growth by inhibition of the x(c)- cystine transporter: a new action for an old drug. Leukemia. 2001; 15(10):1633–1640. [PubMed: 11587223]
27. Dixon SJ, Lemberg KM, Lamprecht MR, Skouta R, Zaitsev EM, Gleason CE, et al. Ferroptosis: an iron-dependent form of nonapoptotic cell death. Cell. 2012; 149(5):1060–1072. [PubMed: 22632970]
28. Yu X, Long YC. Crosstalk between cystine and glutathione is critical for the regulation of amino acid signaling pathways and ferroptosis. Sci Rep. 2016; 6:30033. [PubMed: 27425006]
29. Lukey MJ, Katt WP, Cerione RA. Targeting amino acid metabolism for cancer therapy. Drug discovery today. 2016
30. Lawrence RT, Perez EM, Hernandez D, Miller CP, Haas KM, Irie HY, et al. The proteomic landscape of triple-negative breast cancer. Cell Rep. 2015; 11(4):630–644. [PubMed: 25892236]
31. Harris IS, Treloar AE, Inoue S, Sasaki M, Gorrini C, Lee KC, et al. Glutathione and thioredoxin antioxidant pathways synergize to drive cancer initiation and progression. Cancer Cell. 2015; 27(2):211–222. [PubMed: 25620030]
32. Momcilovic M, Bailey ST, Lee JT, Fishbein MC, Magyar C, Braas D, et al. Targeted Inhibition of EGFR and Glutaminase Induces Metabolic Crisis in EGFR Mutant Lung Cancer. Cell Rep. 2017; 18(3):601–610. [PubMed: 28099841]
33. Muir A, Danai LV, Gui DY, Waingarten CY, Lewis CA, Vander Heiden MG. Environmental cystine drives glutamine anaplerosis and sensitizes cancer cells to glutaminase inhibition. Elife. 2017; 6
34. Davidson SM, Papagiannakopoulos T, Olenchock BA, Heyman JE, Keibler MA, Luengo A, et al. Environment Impacts the Metabolic Dependencies of Ras-Driven Non-Small Cell Lung Cancer. Cell Metab. 2016; 23(3):517–528. [PubMed: 26853747]

35. Prat A, Adamo B, Cheang MC, Anders CK, Carey LA, Perou CM. Molecular characterization of basal-like and non-basal-like triple-negative breast cancer. Oncologist. 2013; 18(2):123–133. [PubMed: 23404817]

36. Azordegan N, Fraser V, Le K, Hillyer LM, Ma DW, Fischer G, et al. Carcinogenesis alters fatty acid profile in breast tissue. Mol Cell Biochem. 2013; 374(1–2):223–232. [PubMed: 23180247]

37. Mohammadzadeh F, Mosayebi G, Montazeri V, Darabi M, Fayezi S, Shaaker M, et al. Fatty Acid Composition of Tissue Cultured Breast Carcinoma and the Effect of Stearoyl-CoA Desaturase 1 Inhibition. J Breast Cancer. 2014; 17(2):136–142. [PubMed: 25013434]

38. Budczies J, Brockmoller SF, Muller BM, Barupal DK, Richter-Ehrenstein C, Kleine-Tebbe A, et al. Comparative metabolomics of estrogen receptor positive and estrogen receptor negative breast cancer: alterations in glutamine and beta-alanine metabolism. Journal of proteomics. 2013; 94:279–288. [PubMed: 24125731]

39. Tang X, Lin CC, Spasojevic I, Iversen ES, Chi JT, Marks JR. A joint analysis of metabolomics and genetics of breast cancer. Breast cancer research : BCR. 2014; 16(4):415. [PubMed: 25091696]

40. Gamcsik MP, Kasibhatla MS, Teeter SD, Colvin OM. Glutathione levels in human tumors. Biomarkers : biochemical indicators of exposure, response, and susceptibility to chemicals. 2012; 17(8):671–691.

41. Lien EC, Lyssiotis CA, Juvekar A, Hu H, Asara JM, Cantley LC, et al. Glutathione biosynthesis is a metabolic vulnerability in PI(3)K/Akt-driven breast cancer. Nat Cell Biol. 2016; 18(5):572–578. [PubMed: 27088857]

42. Timmerman LA, Holton T, Yuneva M, Louie RJ, Padro M, Daemen A, et al. Glutamine sensitivity analysis identifies the xCT antiporter as a common triple-negative breast tumor therapeutic target. Cancer Cell. 2013; 24(4):450–465. [PubMed: 24094812]

43. Trachootham D, Alexandre J, Huang P. Targeting cancer cells by ROS-mediated mechanisms: a radical therapeutic approach? Nature reviews Drug discovery. 2009; 8(7):579–591. [PubMed: 19478820]

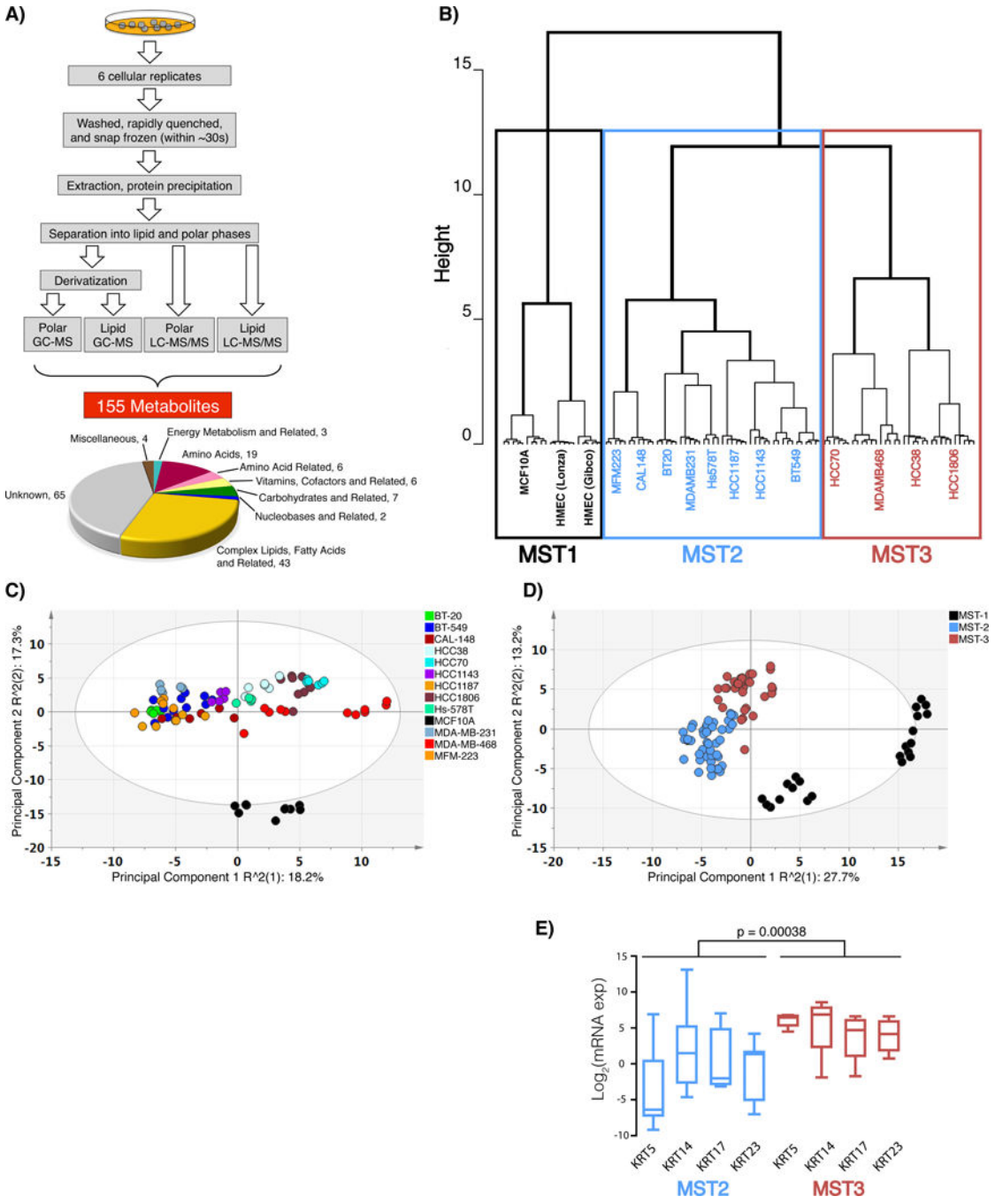

Figure 1. Metabolite profiling reveals three metabolic subtypes (MSTs)

(A) Schematic of metabolite profiling workflow. (B) Unsupervised hierarchical clustering based on the relative levels of 155 intracellular metabolites. Three major MSTs are indicated. A more detailed version with bootstrap analysis of the clusters is available in Fig. S1. (C) PCA plot showing individual cell line replicates. The scores plot for the first two principal components encompasses 18.2% and 17.3% of total variance (13 components calculated in total by SIMCA accounted for 83.4% of the variance). (D) PCA plot of all replicates of all 15 cell lines color-coded by MST. The scores plot for the first two

components encompasses 27.7% and 13.2% of total variance (85.1%; 14 total components in total). Details corresponding to PCA loading of Figure 1C and 1D are given in Table S2. (E) Box and whiskers plots representing mRNA expression of the indicated genes in cell lines of MST2 (blue) and MST3 (red). Whiskers represent the maximum and minimum values. BT-549 was excluded from the comparison for KRT23 because expression was below detection.

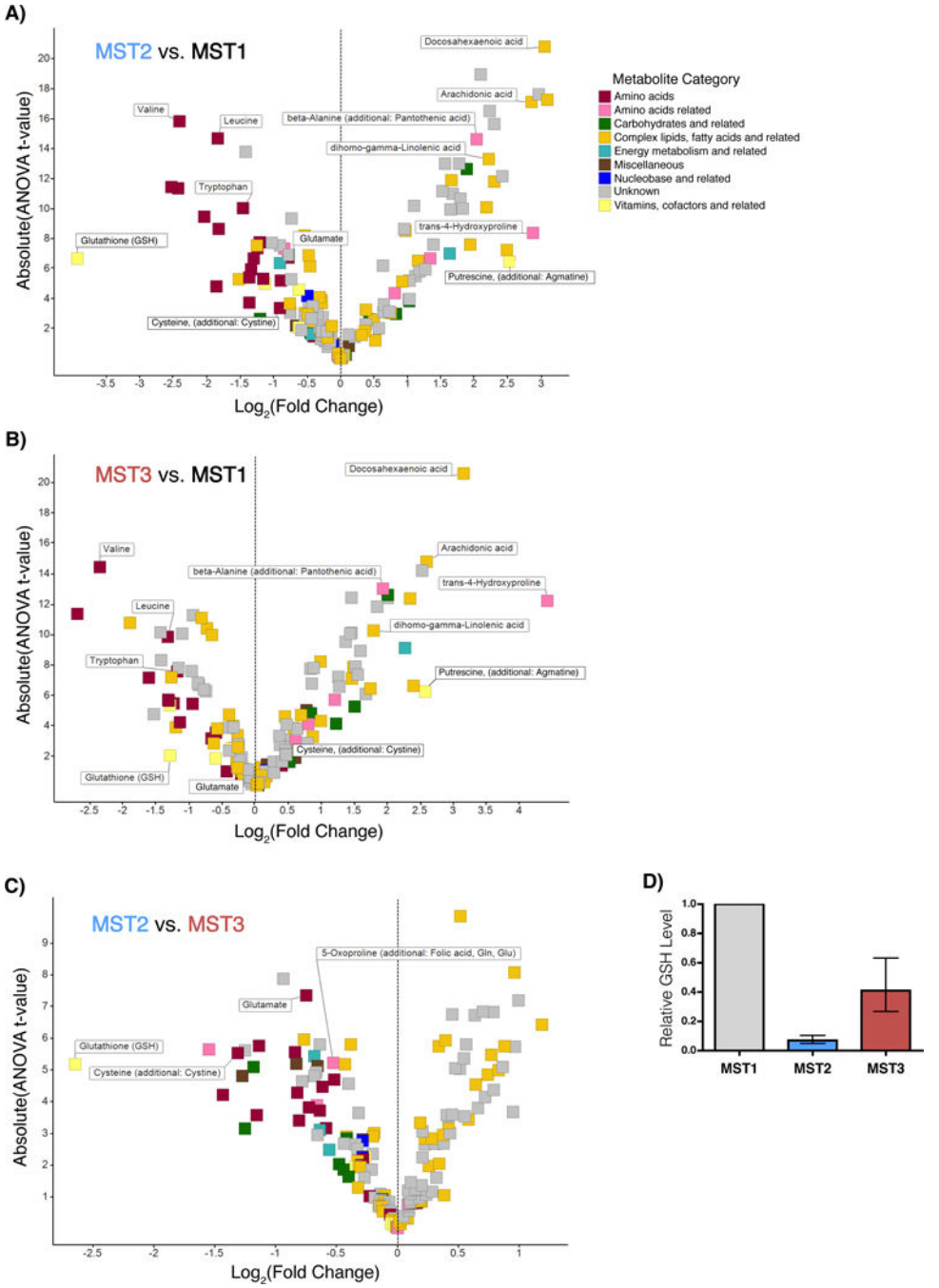

Figure 2. ANOVA analysis identifies metabolites differentially expressed between the metabolic subtypes

Volcano plots displaying the absolute values of the t-values for each of 155 intracellular metabolites from ANOVA analyses versus the $\log_2$-transformed relative fold change for each metabolite for (A) MST1 compared to MST2, (B) MST1 compared to MST3, and (C) MST2 compared to MST3. Metabolites are color coded by metabolite category and selected metabolites are individually labeled. (D) Relative levels of reduced glutathione (GSH) in the three metabolic subtypes. Colors denote MSTs as defined in Figure 1. Error bars represent relative standard deviation.

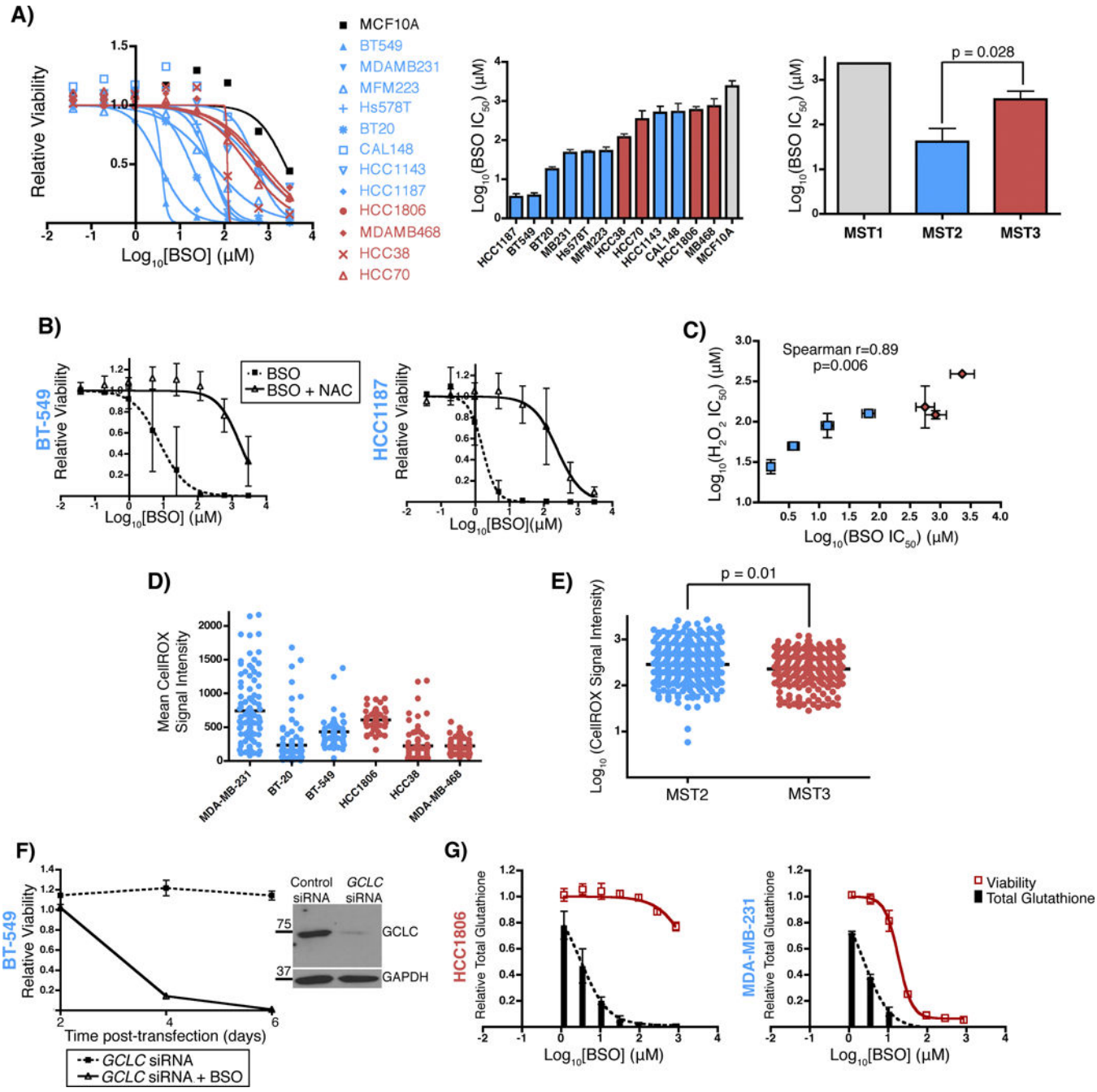

Figure 3. Low glutathione levels reflect increased glutathione consumption in order to reduce reactive oxygen species

(A) BSO dose-response curves showing relative cell viability after 7 days (left), cell lines ranked by BSO IC_{50} value (middle) and comparison of the average BSO IC_{50} value for each MST (right). Errors bars for dose response curves show standard deviation. All other error bars represent standard error of the mean. (B) BSO dose-response curves for two representative cell line of MST2 (BT-549, HCC1187) in the presence or absence of 5 mM N-acetyl cysteine (NAC). (C) Scatter plot of log-transformed IC_{50} values for BSO versus log-transformed IC_{50} for H_2O_2 in cell viability assays for representative members of MST2

(HCC1187, BT-549, BT-20, MDA-MB-231), colored blue, and of MST3 (HCC70, HCC1806, MDA-MB-468), colored red. The Spearman r and associated p-value from a Spearman correlation are shown. The BSO IC_{50} values correspond to those reported in Panel A. (D) Cellular ROS levels were measured by CellROX for individual cells of each specified type and are grouped by MST in (E). (F) Relative viability of BT-549 cells after siRNA knockdown of GCLC in the presence or absence of a sub-lethal dose of BSO (1 μM). Western blots show knockdown of GCLC 72 hours after transfection. GAPDH serves as a loading control. (G) BSO dose-response curves showing relative cell viability and relative glutathione levels (black; oxidized plus reduced forms) after 72 hours of treatment for the indicated cell lines.

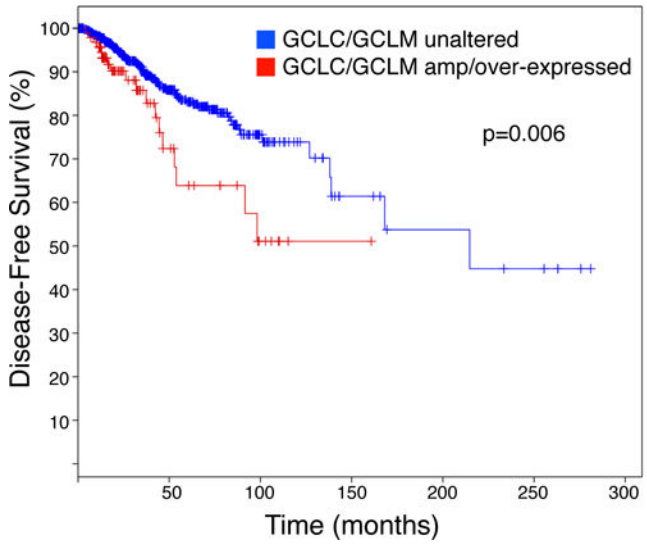

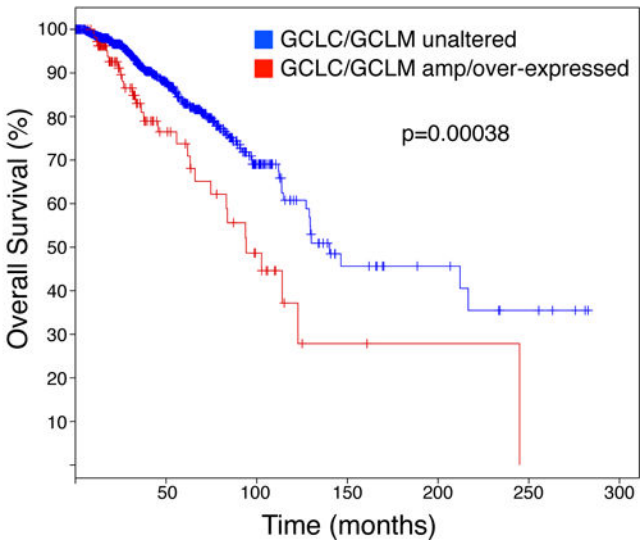

Figure 4. *GCLC/GCLM* overexpression or amplification is associated with worse progression-free and overall survival in breast cancer patients

Kaplan-Meier curves showing disease-free survival (left) and overall survival (right) in breast cancer patients included in the provisional TCGA invasive breast carcinoma dataset. Data was analyzed using cBioportal and a z-score threshold of ±2.0.

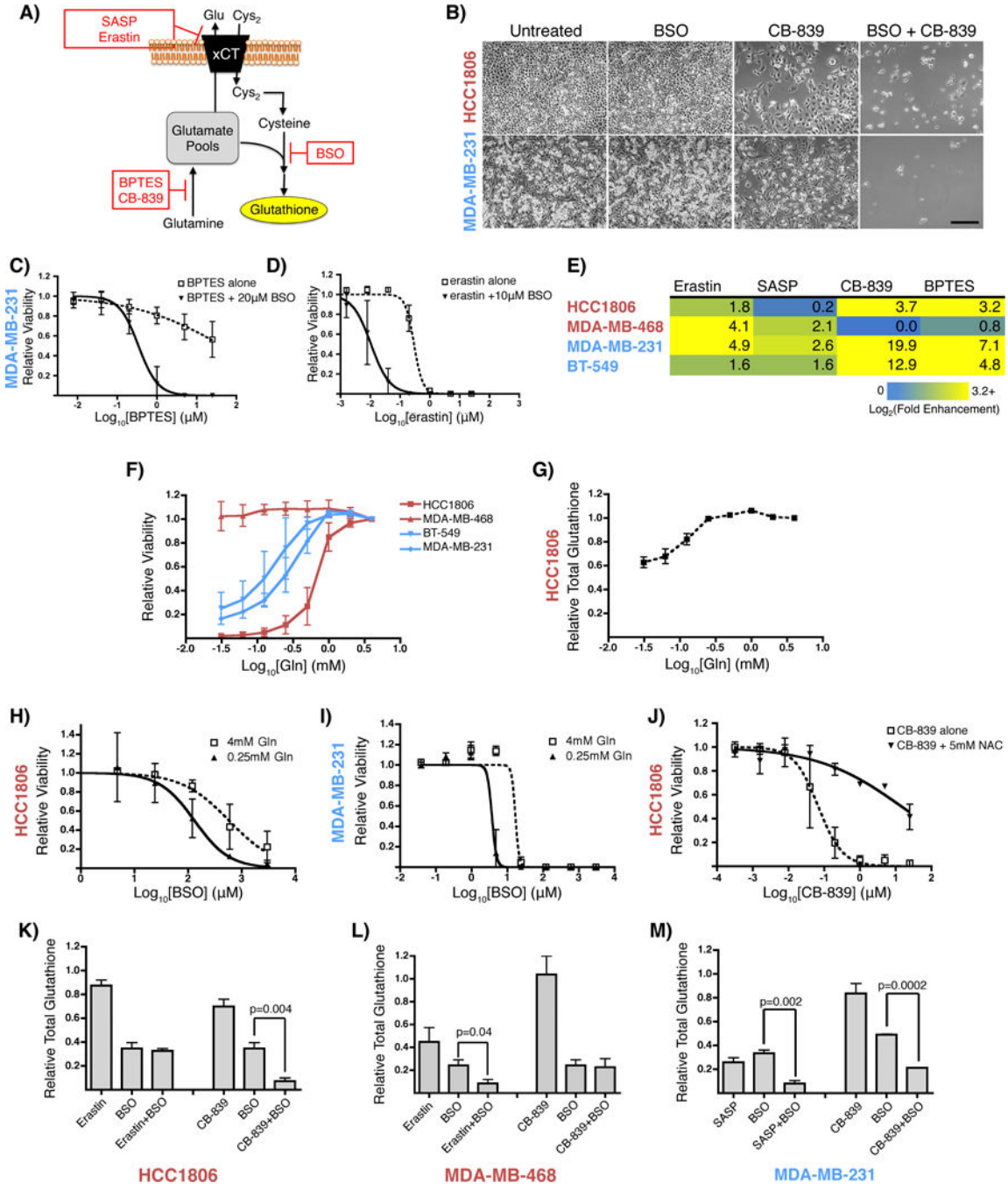

Figure 5. Treatment combinations that limit glutathione biosynthesis inhibit TNBC cell growth

(A) Schematic representation of druggable metabolic pathways involved in glutathione biosynthesis. (B) Light micrographs of HCC1806 (top) or MDA-MB-231 (bottom) treated as indicated for 7 days. The dose of CB-839 was 200 nM and BSO dose was 40 μM for HCC1806 and 10 μM for MDA-MB-231. Scale bar represents 200 μm. Dose-response curves showing relative cell viability versus dose of (C) BPTES or (D) erastin in the presence or absence of a sub-toxic dose of BSO. (E) Heat map showing fold-enhancement of growth suppression by the indicated inhibitor in the presence of BSO. The values correspond

to the $\log_2$-transformed ratio of the IC_{50} of each agent in CellTiter-Glo cell viability assays divided by its IC_{50} in the presence of a sensitizing dose of BSO (Fig. S5A & S5B). Positive values denote enhancement of toxicity. F) Cell viability of the indicated cell lines after culturing for 7 days in media containing the indicated concentration of glutamine. (G) Relative levels of total glutathione after culturing HCC1806 cells for 24 hours in media containing the specified concentration of glutamine. (H) and (I) show relative cell viability of cell cultures after growing for 7 days with the indicated concentration of BSO and either high or low glutamine, as shown. J) Dose-dependent effect of CB-839 on the viability of HCC1806 cells in the absence or presence of N-acetylcysteine. Relative total glutathione levels after 24 hour of treatment of (K) HCC1806, (L) MDA-MB-468, or (M) MDA-MB-231 with the designated agents. For (K) and (L), doses of BSO, erastin, and CB-839 were 8 μM, 200 nM, and 40 nM, respectively. For (M), BSO plus SASP, 5 μM BSO and 200 μM SASP were used, while for BSO plus CB-839, 1 μM BSO and 40 nM CB-839 were used.

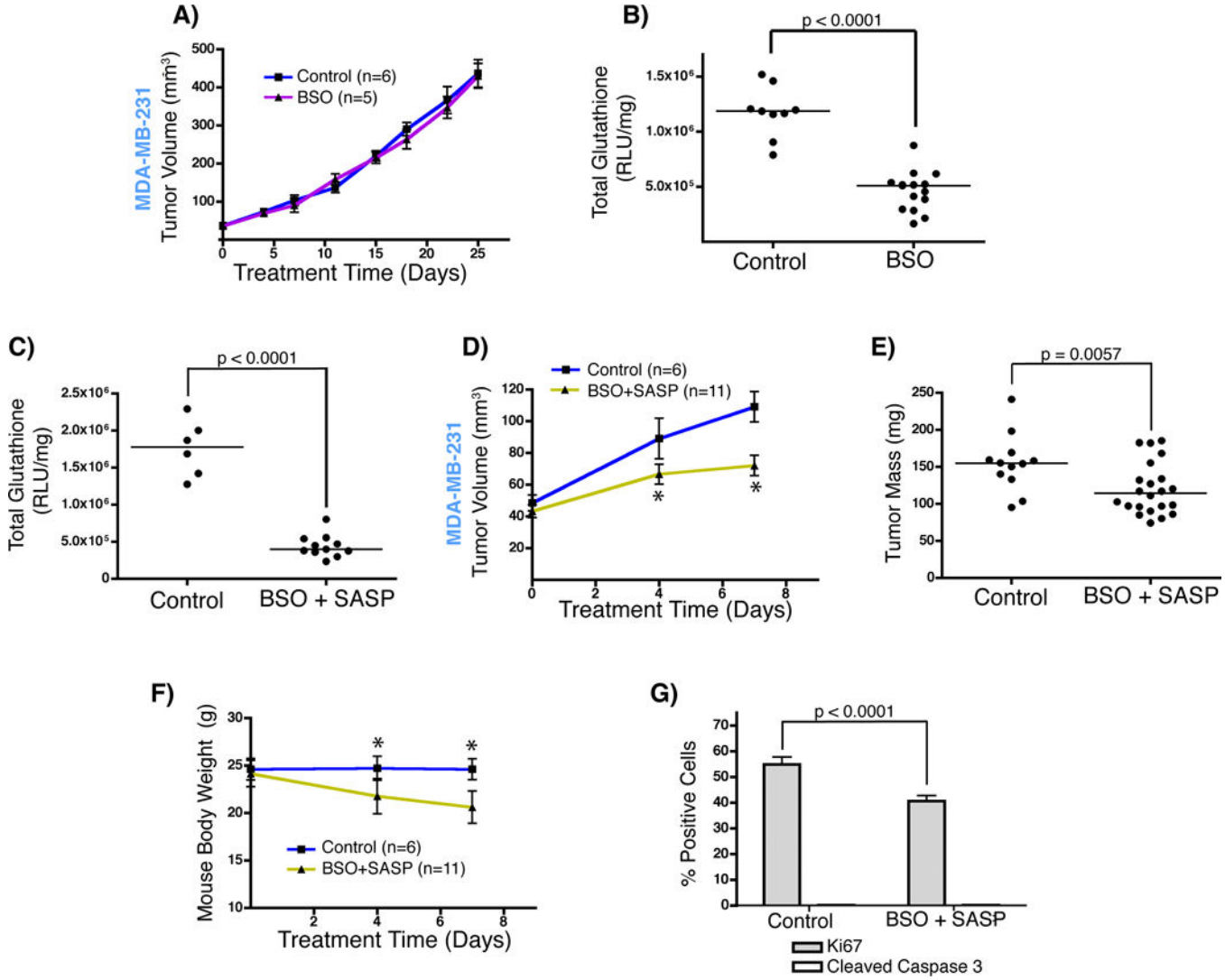

Figure 6. Treatment combinations limit glutathione biosynthesis *in vivo*

(A) Median tumor volume over time for mice treated with 20 mM BSO in the drinking water or control water. (B) Masses of the tumors in (A) following dissection at the end of the study. (C) Total glutathione measured from lysates of tumors treated with BSO in combination with SASP or with vehicle alone. One tumor was analyzed from each mouse. Corresponding tumor growth is shown in (D) and final tumor masses in (E) for all tumors. A larger number of mice was used in the treatment group due to anticipated toxicity though only one mouse was culled for significant body weight loss and was excluded from the data. Lines represent the median values. (F) Mean body weights of mice measured over the treatment period in (D). (G) Percentage of Ki-67-positive or caspase 3-positive cells (less than 0.2% in either condition) in MDA-MB-231 tumor sections.